

Spin-triplet paired phases inside a ferromagnet induced by Hund's rule coupling and electronic correlations: Application to UGe_2

E. Kądziaława-Major,^{1,*} M. Fidrysiak,^{1,†} P. Kubiczek,^{2,‡} and J. Spalek^{1,§}

¹Marian Smoluchowski Institute of Physics, Jagiellonian University, ulica Łojasiewicza 11, 30-348 Kraków, Poland

²I. Institut für Theoretische Physik, Universität Hamburg, Jungiusstraße 9, D-20355 Hamburg, Germany



(Received 21 December 2017; revised manuscript received 5 June 2018; published 25 June 2018)

We discuss a mechanism of real-space spin-triplet pairing, which is an alternative to the one due to quantum paramagnon excitations, and demonstrate its applicability to UGe_2 . Both the Hund's rule ferromagnetic exchange and interelectronic correlations contribute to the same extent to the equal-spin pairing, particularly in the regime where the weak-coupling solution does not provide any. The theoretical results, obtained within the orbitally degenerate Anderson lattice model, excellently match the observed phase diagram for UGe_2 with the coexistent ferromagnetic (FM1) and superconducting (A_1 -type) phases. Additionally, weak A_2 - and A -type paired phases appear in very narrow regions near the metamagnetic (FM2 \rightarrow FM1) and FM1 to paramagnetic first-order phase-transition borders, respectively. The values of magnetic moments in the FM2 and FM1 states are also reproduced correctly in a semiquantitative manner. The Hund's metal regime is also singled out as appearing near the FM1-FM2 boundary.

DOI: [10.1103/PhysRevB.97.224519](https://doi.org/10.1103/PhysRevB.97.224519)

I. INTRODUCTION

The discovery of superconductivity (SC) in uranium compounds UGe_2 [1–4], URhGe [5], UCoGe [6], and UIr [7] that appears inside the ferromagnetic (FM) phase but close to magnetic instabilities has reinvented the principal question concerning the mechanism of the spin-triplet pairing. The latter is particularly intriguing since the spin-triplet SC [8–11] occurs relatively seldom in correlated systems compared to its spin-singlet analog. More importantly, the case where the paired state in both UGe_2 and UIr is absent on the paramagnetic (PM) side of the FM1 \rightarrow PM discontinuous transition suggests a specific mechanism providing, on the same footing, both the magnetic and SC orderings. Moreover, SC is well established in one particular (FM1) magnetic phase but not in the FM2 and PM phases, where the magnetic moment is either almost saturated or vanishes, respectively. These circumstances pose a stringent test on any pairing mechanism which should be tightly connected to the onset/disappearance of ferromagnetism.

The spin-triplet SC mediated by quantum spin fluctuations has been invoked [12,13] and tested for UCoGe [14–16], which represents systems with very low magnetic moments [14,17] ($m \sim 0.039\mu_B/\text{U}$) and thus is particularly amenable to the fluctuations in both the weakly ordered FM and PM regimes. From this perspective, UGe_2 possesses a large magnetic moment in the FM1 phase ($m \sim 1\mu_B/\text{U}$), and in the low-pressure FM2 phase it is even larger ($m \sim 1.5\mu_B/\text{U}$) [3]. In such a situation, a natural idea arises that in this case local

correlation effects should become much more pronounced in UGe_2 , particularly because the dominant SC phase appears in between two metamagnetic transitions, one of which (FM2 \rightarrow FM1) can be associated with the transition from the almost localized FM2 phase of $5f$ electrons. Closely related to this is the question of the applicability of real-space spin-triplet pairing, considered before as being relevant to the orbitally degenerate correlated narrow-band systems [18–26], which in turn is analogous to the spin-singlet pairing proposed for the high-temperature [27–32] and heavy-fermion [33–36] superconductors. Essentially, we explore the regime of large and weakly fluctuating moments. The relevance of this idea is supported by the recent experimental evidence that the ratio of spontaneous moment m to its fluctuating counterpart m_0 is ~ 1 , whereas for UCoGe , $m_0 \gg m$, so the two systems are located on opposite sides of the Rhodes-Wohlfarth plot [37].

Explicitly, we put forward the idea of correlation-induced pairing and test it for the case of UGe_2 . To implement that program we generalize our approach, applied earlier [38–40] to explain the magnetic properties of UGe_2 , and incorporate this specific type of coexistent SC into that picture. Specifically, we extend the spin-triplet pairing concepts, originally introduced for the case of multiorbital narrow-band systems [18–24], by including the Hund's rule coupling combined with intra-atomic correlations within the orbitally degenerate Anderson lattice model (ALM) and treat it within the statistically consistent version of the renormalized mean-field theory (the statistically consistent Gutzwiller approximation, SGA) [38–40]. In this manner, we demonstrate, in quantitative terms, the applicability of the concept of even-parity, spin-triplet pairing to UGe_2 . Furthermore, we also provide a detailed analysis of the two very narrow border regions, FM2-FM1 and FM1-PM, in which a weak A_2 -type SC transforms to A_1 and from A_1 to the practically marginal A phase, respectively, before

*ewa.kadzielawa@doctoral.uj.edu.pl

†maciej.fidrysiak@uj.edu.pl

‡patryk.kubiczek@physik.uni-hamburg.de

§jozef.spalek@uj.edu.pl

SC disappears altogether (the notation of the SC phases is analogous [41] to that used for superfluid ^3He).

The present mechanism may be regarded as complementary to the reciprocal-space pairing by long-wavelength quantum spin fluctuations, which was very successful in explaining the properties of the superfluid ^3He [42,43]. The latter mechanism was also applied to ferromagnets with magnetic-moment fluctuations on both the weakly FM and PM sides [44,45]. Specifically, the role of their longitudinal component was emphasized. However, all those considerations have been limited to a single-band situation, and therefore, SC is unavoidably of p -wave character. The multiband structure, considered here, allows for an even-parity SC state which can take the form of an s wave.

II. MODEL AND METHOD

We start with doubly degenerate f states and assume a two-dimensional structure of the compound [46,47]. Within our model, the total number of electrons per formula unit $n^{\text{tot}} \equiv n^f + n^c$, with n^f and n^c being the f and conduction (c) electron occupancies, must exceed that on the $5f$ level for a U^{3+} ion [8,48,49], i.e., $n > 3$. The best comparison with experiment is achieved here for $n^{\text{tot}} \simeq 3.25$. This presumption brings into mind the idea of an orbitally selective delocalization of one out of the three $5f$ electrons under pressure (see below).

Explicitly, we employ a four-orbital ALM defined by the Hamiltonian (with the chemical potential term $-\mu\hat{N}_e$ included)

$$\begin{aligned} \mathcal{H} - \mu\hat{N}_e &= \sum_{ijl\sigma} t_{ij} \hat{c}_{i\sigma}^{(l)\dagger} \hat{c}_{j\sigma}^{(l)} + V \sum_{i\sigma} (\hat{f}_{i\sigma}^{(1)\dagger} \hat{c}_{i\sigma}^{(l)} + \text{H.c.}) \\ &+ \epsilon^f \sum_{il} \hat{n}_i^{f(l)} + U \sum_{il} \hat{n}_{i\uparrow}^{f(l)} \hat{n}_{i\downarrow}^{f(l)} + U' \sum_i \hat{n}_i^{f(1)} \hat{n}_i^{f(2)} \\ &- 2J \sum_i \left(\hat{\mathbf{S}}_i^{f(1)} \cdot \hat{\mathbf{S}}_i^{f(2)} + \frac{1}{4} \hat{n}_i^{f(1)} \hat{n}_i^{f(2)} \right) - \mu\hat{N}_e, \quad (1) \end{aligned}$$

involving two f orbitals (with creation operators $\hat{f}_{i\sigma}^{(l)\dagger}$, with $l = 1, 2$ at lattice site i and spin $\sigma = \uparrow, \downarrow$), hybridized with two species of conduction electrons created by $\hat{c}_{i\sigma}^{(l)\dagger}$ (minimally, two c bands are needed because, otherwise, one of the f orbitals decouples and does not participate in the resultant quasiparticle states [50]). Out of general hopping matrix t_{ij} we retain nearest- and next-nearest-neighbor hoppings (t, t') and assume a local character of f - c hybridization V . Correlations in the f -electron sector are governed by intraorbital f - f repulsion U , interorbital repulsion U' , and Hund's coupling J . Here $\hat{n}_i^{f(l)}$ and $\hat{\mathbf{S}}_i^{f(l)}$ denote the f -electron number and spin operators on site i for orbital l , whereas \hat{N}_e is the total particle number. Hereafter, we restrict ourselves to the case of $U' = U - 2J$, $U/|t| = 3.5$, and $t'/|t| = 0.25$. The values of parameters have been selected to reproduce correctly the observed values of magnetic moments, the magnetic critical points [39], and the maximal value of the SC transition temperature $T_{\text{SC}} \lesssim 1$ K, all at the same time. Also, we neglect the interorbital pair-hopping term $\sim J$ as it contributes only to the spin-singlet pairing channel.

The SGA approach is based on optimization of the ground-state energy within the class of wave functions with partially projected out double- f -orbital occupancies and can be formulated in terms of the effective one-body Hamiltonian

$$\mathcal{H}_{\text{eff}} = \sum_{\mathbf{k}, \sigma} \Psi_{\mathbf{k}\sigma}^\dagger \begin{pmatrix} \epsilon_{\mathbf{k}} & 0 & q_\sigma V & 0 \\ 0 & -\epsilon_{\mathbf{k}} & 0 & -q_\sigma V \\ q_\sigma V & 0 & \epsilon_\sigma^f & \Delta_{\sigma\sigma}^{ff} \\ 0 & -q_\sigma V & \Delta_{\sigma\sigma}^{ff} & -\epsilon_\sigma^f \end{pmatrix} \Psi_{\mathbf{k}\sigma} + E_0, \quad (2)$$

derived from the model of Eq. (1) (see Appendix A). In Eq. (2) $\Psi_{\mathbf{k}\sigma}^\dagger \equiv (\hat{c}_{\mathbf{k}\sigma}^{(1)\dagger}, \hat{c}_{-\mathbf{k}\sigma}^{(2)\dagger}, \hat{f}_{\mathbf{k}\sigma}^{(1)\dagger}, \hat{f}_{-\mathbf{k}\sigma}^{(2)\dagger})$, $\epsilon_{\mathbf{k}}$ denotes the bare c -electron dispersion relation, ϵ_σ^f is an effective f level, $\Delta_{\sigma\sigma}^{ff} \equiv \mathcal{V}_\sigma \langle \hat{f}_{i\sigma}^{(1)} \hat{f}_{i\sigma}^{(2)} \rangle$ is the f - f equal-spin SC gap parameter, $\mathcal{V}_\sigma \equiv -U'g_{1\sigma} + (J - U')g_{2\sigma}$ denotes the effective pairing coupling, and E_0 is a constant. The renormalization factors q_σ , $g_{1\sigma}$, and $g_{2\sigma}$ account for the correlation effects and originate from the projection of the trial wave functions (see Appendix A for explicit expressions).

The basic quantity determined from the diagonalization of \mathcal{H}_{eff} (see Appendix A) is the quasiparticle gap $\Delta_{\mathbf{k}}$. For wave vectors lying on the Fermi surface of the normal state, one obtains

$$\Delta_{\mathbf{k}}^2 = \frac{\epsilon_{\mathbf{k}}^2}{(\epsilon_{\mathbf{k}} + \epsilon_\sigma^f)^2} (\Delta_{\sigma\sigma}^{ff})^2 + o[(\Delta_{\sigma\sigma}^{ff})^2], \quad (3)$$

so $\Delta_{\mathbf{k}}$ is expressed in terms $\Delta_{\sigma\sigma}^{ff}$ and a weakly \mathbf{k} dependent factor. Therefore, in the remaining discussion we use the latter gap, underlining in this manner the dominant role of the f - f pairing.

The quantity particularly relevant to the present discussion is the equal-spin coupling constant \mathcal{V}_σ . If positive, this term favors equal-spin-triplet SC. We also define the Hartree-Fock (HF/BCS) coupling constant $\mathcal{V}_{\text{HF}} = J - U'$, independent of the spin direction. In the latter approximation the interatomic interaction is attractive when $J - U' = 3J - U > 0$ (this condition defines the BCS limit). One of the principal signatures of correlation importance is that pairing persists even when the coupling \mathcal{V}_{HF} becomes *repulsive* ($\mathcal{V}_{\text{HF}} < 0$), as shown below. The conditions $\mathcal{V}_{\text{HF}} < 0$ and $\mathcal{V}_\sigma > 0$ define the regime of correlation-driven SC.

III. RESULTS

The complete phase diagram encompassing both the FM and SC states for selection of Hund's coupling $J/|t| = 1.1$ is shown in Fig. 1 (see Appendixes B and C for technical aspects of the analysis). In Fig. 1(a) we illustrate the system evolution from the large-moment FM2 phase through the FM1 state with a magnetization plateau at $\sim 0.8\mu_B$ (compared to $\sim 1\mu_B$ measured for UGe_2 [3]) to the PM phase as the hybridization magnitude $|V|$ increases. Here changing $|V|$ mimics its pressure variation. Both the $\text{FM2} \rightarrow \text{FM1}$ and $\text{FM1} \rightarrow \text{PM}$ transitions are of the first order, as is observed for UGe_2 below the critical end point, although the $\text{FM2} \rightarrow \text{FM1}$ transition is of weak first order due to the proximity to the quantum tricritical point [39] [see Fig. 1(d)]. Notably, our

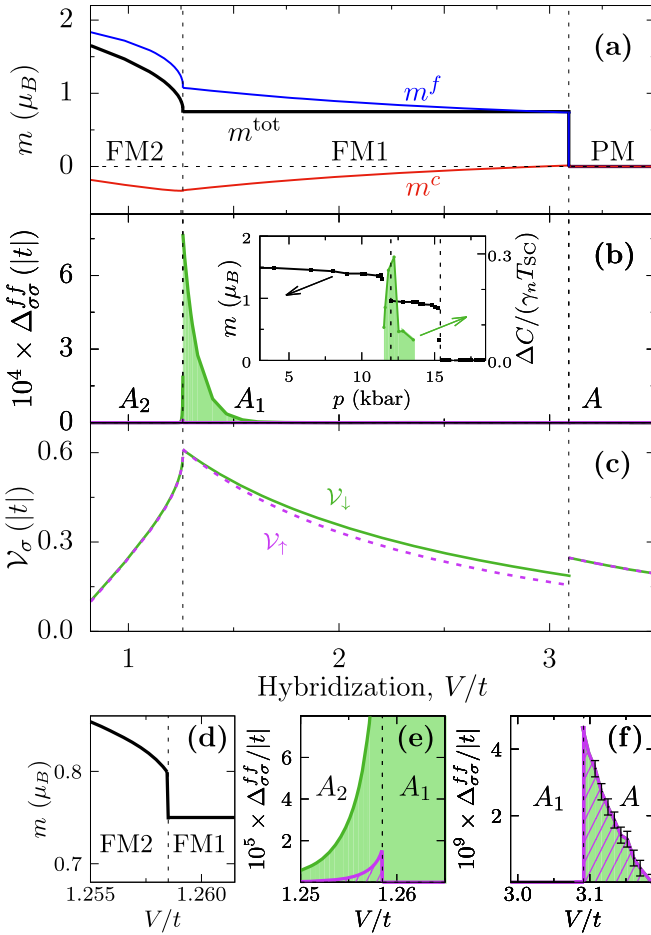


FIG. 1. Calculated zero-temperature phase diagram of UGe_2 for Hund's coupling $J/|t| = 1.1$ versus f - c hybridization V . The remaining parameters read $t'/|t| = 0.25$, $U/|t| = 3.5$, $\epsilon^f/|t| = -4$, and $n^{\text{tot}} = 3.25$. (a) Total magnetic moment m^{tot} per formula unit (black solid line) and the corresponding f and c electron magnetizations, m^f and m^c (blue and red lines, respectively). m^c represents a residual Kondo compensating cloud. (b) Triplet f - f SC gap component $\Delta_{\uparrow\uparrow}^{ff}$ (purple shading) and $\Delta_{\downarrow\downarrow}^{ff}$ (green shading). Three distinct SC phases, A_2 , A_1 , and A , are marked. The A -phase gaps ($\sim 10^{-9}|t|$) are not visible. The inset shows experimental magnetization for UGe_2 [3] and the specific-heat jump at the SC transition temperature T_{SC} (normalized by T_{SC} and the linear specific-heat coefficient γ_n) [51]. (c) Effective coupling constant \mathcal{V}_σ for spin-up (purple) and spin-down (green) triplet pairing. Note that the value of coupling is largest near the $A_2 \rightarrow A_1$ transition. (d) Total magnetic moment near the FM2 \rightarrow FM1 metamagnetic transition. (e) and (f) SC gap components near the FM2 \rightarrow FM1 and FM1 \rightarrow PM transition points, respectively.

model also provides the value of magnetic moment $m \sim 1.6\mu_B$ in the FM2 phase, close to the experimental $m \approx 1.45\mu_B$ [3].

The unique feature, inherent to the degenerate ALM and the principal result of the present paper, is the emergence of distinct even-parity spin-triplet SC phases around the magnetic transition points, characterized by nonzero SC gap parameters $\Delta_{\sigma\sigma}^{ff} \equiv \mathcal{V}_\sigma \langle \hat{f}_{i\sigma}^{(1)} \hat{f}_{i\sigma}^{(2)} \rangle_0$, as depicted in Fig. 1(b). The A_1 -type SC (i.e., the majority-spin gap $\Delta_{\uparrow\uparrow}^{ff} = 0$ and $\Delta_{\downarrow\downarrow}^{ff} \neq 0$) sets in inside the FM1 phase and transforms to either the A_2 phase ($\Delta_{\downarrow\downarrow}^{ff} > \Delta_{\uparrow\uparrow}^{ff} \neq 0$) at the FM2-FM1 border or to the

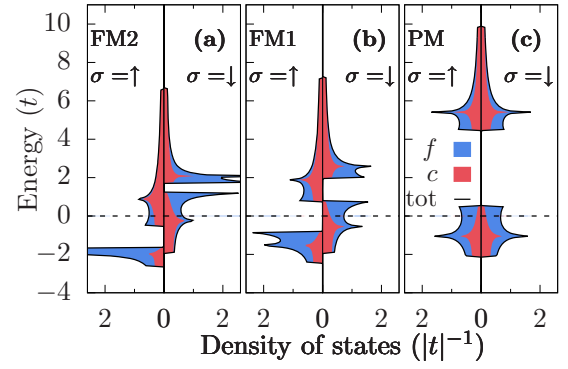


FIG. 2. Spin- and orbital-resolved density of states for $J/|t| = 1.1$ in the (a) FM2 ($V/t = 1.1$), (b) FM1 ($V/t = 1.625$), and (c) PM ($V/t = 3.25$) phases. Orbital contributions are marked in blue and red, whereas the total density of states is plotted by the black solid line. Dirac δ functions have been smeared out by $\epsilon = 10^{-3}|t|$ for numerical purposes.

A state ($\Delta_{\uparrow\uparrow}^{ff} = \Delta_{\downarrow\downarrow}^{ff} \neq 0$) close to the FM1 \rightarrow PM transition point. The latter two states appear in very narrow regions, as illustrated in Figs. 1(e) and 1(f). The A_2 -phase gap is, by an order of magnitude, smaller than its A_1 counterpart, whereas the A -phase gap is, by four orders of magnitude, even smaller. Hence, one can safely say that the A_1 phase is so far the only one observable for UGe_2 ; the A_2 state could be detectable in applied magnetic field [52]. Note also that the pairing potential \mathcal{V}_\downarrow is maximal near the corresponding metamagnetic transition [see Fig. 1(c)]. Remarkably, this situation appears without any additional spin-fluctuation effect involved, which distinguishes the present mechanism from those invoked previously for the U compounds [13–15]. In the inset of Fig. 1(b), we plot the specific-heat discontinuity (the shaded area) and the related magnetization jumps observed experimentally. The peaks identify the regime of bulk SC; these sharp features are reproduced by our calculation [see Fig. 1(b)] and should be contrasted with the first resistivity data [1]. Note also that we obtain small, but clear, SC gap discontinuities at both the $A_2 \rightarrow A_1$ and $A_1 \rightarrow A$ transitions [see Fig. 1(e) and 1(f), respectively]. We emphasize that all the singularities are physically meaningful and well within the numerical accuracy (error bars are shown explicitly for the A phase with the smallest gap magnitude).

The nature of the FM2 and FM1 phases can be understood by inspecting the corresponding spin- and orbital-resolved densities of states shown in Fig. 2. In the FM2 state [Fig. 2(a)] f electrons are close to localization and well below the Fermi energy ϵ_F as they carry out nearly saturated magnetic moments, whereas in the FM1 phase [Fig. 2(b)] ϵ_F is placed in the region of spin-down electrons, stabilizing the magnetization plateau (and illustrating the *half-metallic character*); hence, only $\Delta_{\downarrow\downarrow}^{ff} \neq 0$. A similar evolution of magnetism was observed previously for the orbitally nondegenerate model [38–40]. Figure 2(c) illustrates the paramagnetic behavior.

Next, we discuss the fundamental role of the effective pairing potential. Explicitly, in Fig. 3(a) we plot renormalized and bare coupling constants as a function of J for $V/t = 1.32$. The dominant component \mathcal{V}_\downarrow remains positive down to $J/|t| \approx 0.76$, whereas the HF/BCS coupling changes sign

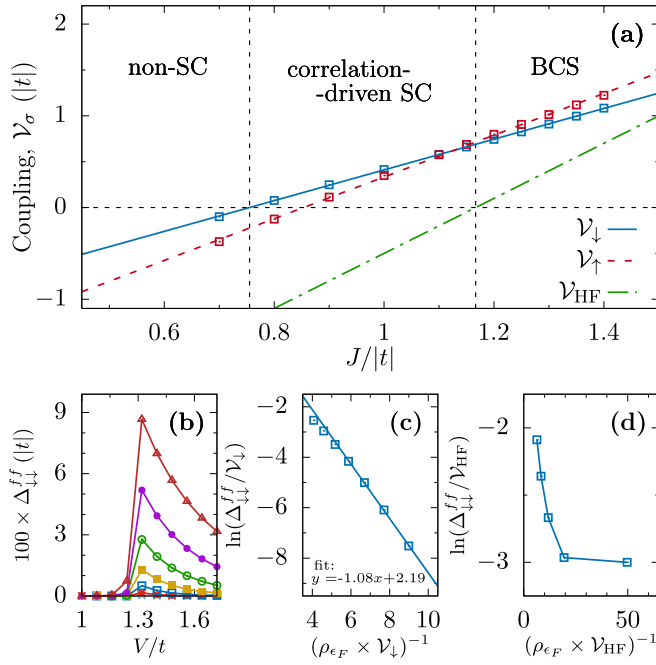


FIG. 3. (a) Dependence of \mathcal{V}_σ on the Hund's coupling J for $V/t = 1.32$ (solid blue and dashed red lines). For comparison, the value of the Hartree-Fock (HF/BCS) coupling constant \mathcal{V}_{HF} is also shown by the green dash-dotted line. Black dashed vertical lines split the plot into three regions: non-SC, correlation-driven (where SC is not supported at the HF/BCS level yet appears due to correlation effects), and BCS (where the SC phase emerges in the HF/BCS approximation) regimes. Note that the value $J/|t| = 1.1$, considered above, falls into the correlation-driven regime. (b) Hybridization dependence of the SC gap component $\Delta_{\downarrow\downarrow}^{ff}$ for various J near the FM2 \rightarrow FM1 transition. Values of $J/|t|$ (from top to bottom) are 1.4, 1.35, 1.3, 1.25, 1.2, 1.15, and 1.1. (c) Scaling of $\Delta_{\downarrow\downarrow}^{ff}$ with the dimensionless effective coupling $\rho_{\epsilon_F} \mathcal{V}_\downarrow$. Here ρ_{ϵ_F} denotes the total density of states per f orbital per spin, evaluated at the Fermi energy in the normal phase. The gap follows renormalized BCS scaling $\Delta_{\downarrow\downarrow}^{ff} \propto \mathcal{V}_\downarrow \times \exp[-(\rho_{\epsilon_F} \mathcal{V}_\downarrow)^{-1}]$. (d) The same as in (c), but with HF/BCS coupling \mathcal{V}_{HF} used instead of \mathcal{V}_\downarrow . Breakdown of BCS scaling implies the relevance of the correlation-driven coupling renormalization.

already for $J/|t| = 3.5/3 \approx 1.17$. Electronic correlations are thus the crucial factor stabilizing the triplet SC close to the FM2-FM1 boundary. Figure 3(b) shows the dominant gap component for selected values of J . The gap increases very rapidly with the increasing Hund's rule coupling, as detailed in Fig. 3(c), where we plot the logarithm of the normalized gap $\ln(\Delta_{\downarrow\downarrow}^{ff}/\mathcal{V}_\downarrow)$ vs $(\rho_{\epsilon_F} \mathcal{V}_\downarrow)^{-1}$ for fixed hybridization $V/t = 1.32$, which corresponds to the A_1 phase (ρ_{ϵ_F} is the total density of states per f orbital per spin at ϵ_F). A good linear scaling is observed with the coefficient ≈ -1.08 , not too far from the BCS value of -1 . The binding of f electrons into local triplet pairs is provided partly by the Hund's rule exchange that yields the HF/BCS potential $\mathcal{V}_{\text{HF}} = 3J - U$. Figure 3(d) is the same as Fig. 3(c), but \mathcal{V}_{HF} has been taken in place of \mathcal{V}_\downarrow . The breakdown of the scaling implies a significant effect of local correlations on the Hund's-rule-induced pairing. The relevance of the local Coulomb interactions combined with the Hund's rule physics can also be seen by comparing the contributions

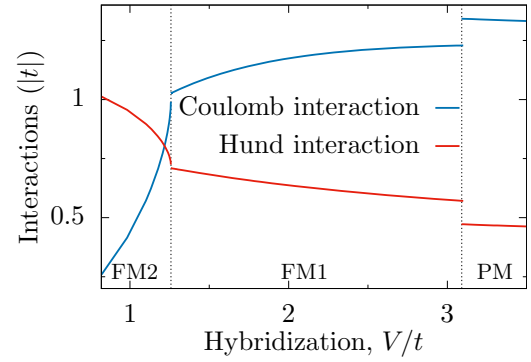


FIG. 4. Comparison of the intraorbital Coulomb and Hund's rule coupling contributions to the total system energy as a function of the hybridization magnitude V/t . These two quantities are defined as $2U \langle \hat{n}_{i\uparrow}^{f(1)} \hat{n}_{i\downarrow}^{f(1)} \rangle_{\text{G}}$ and $2J \langle (\hat{\mathbf{S}}_i^{f(1)} \cdot \hat{\mathbf{S}}_i^{f(2)} + \frac{1}{4} \hat{n}_i^{f(1)} \hat{n}_i^{f(2)}) \rangle_{\text{G}}$, respectively. The two energies are comparable near the FM2 \rightarrow FM1 borderline, which is hence called the Hund's metal regime (see the main text).

of the intraorbital Coulomb repulsion and interorbital Hund's rule coupling to the total ground-state energy (Fig. 4). Close to the metamagnetic FM2 \rightarrow FM1 transition, where the SC amplitude is the largest, those two scales are comparable and of the order of the kinetic term $|t|$. This places the system in the correlated *Hund's metal regime*, previously coined in the context of Fe-based SC [53].

IV. DISCUSSION AND CONCLUSIONS

To underline the quantitative aspect of our analysis of the SC phase we have determined the temperature dependence of the gap in the combined FM1 + A_1 state for $J/|t| = 1.1$ and $V/t = 1.3$, i.e., near the gap-maximum point depicted in Fig. 1(b). Selecting the value of $|t| = 0.5$ eV, we obtained the SC critical temperature $T_{\text{SC}} \approx 0.92$ K (see Appendix D), very close to the experimental value $T_{\text{SC}} \sim 0.75$ K in the highest-quality samples [54]. Note that for $J \lesssim 1.17|t|$ we do not expect any SC in the HF/BCS approximation. It is gratifying that the value of $J = 1.1|t| = 0.55$ eV can lead to such a subtle SC temperature scale $T_{\text{SC}} < 1$ K in the situation where the FM transition temperature T_c is larger by two orders of magnitude or even higher. Equally important is the obtained value of the specific-heat jump $\Delta C/(\gamma_n T_{\text{SC}}) \simeq 1.44$ (see Fig. 8), i.e., very close to the BCS value of 1.43. Parenthetically, this is not too far from experimental $\Delta C/(\gamma_n - \gamma_0)/T_{\text{SC}} \simeq 0.97$ for a pressure of 1.22 GPa [51] (corresponding closely to our choice of parameters) if we subtract the residual Sommerfeld coefficient γ_0 .

The U^{3+} ionic configuration is $5f^3$. Some experimental evidence points to the value close to U^{4+} ($5f^2$) [8,48]. Here the good values of magnetic moments in both the FM2 and FM1 phases were obtained for the approximate $5f^2$ configuration and $n^c \approx 1.25$ conduction electrons, as shown in Fig. 5(a). Namely, the results in Fig. 5(b) point clearly to the value $n^f \approx 2$ in the FM2 phase, and it diminishes almost linearly in the FM1 state. Such a behavior explains that the two f electrons are practically localized in the FM2 phase, and therefore, no SC state induced by the Hund's rule and f - f correlations can be expected. On the other hand, the correlations are weaker on

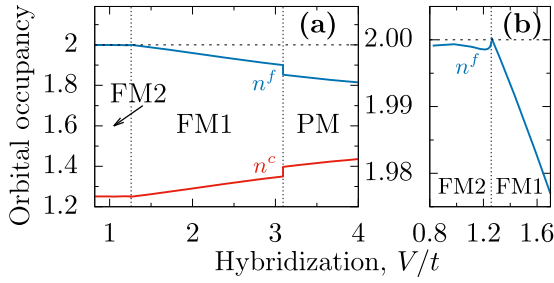


FIG. 5. (a) Occupancies of the f and c orbitals as a function of hybridization. (b) Close-up of the FM2 \rightarrow FM1 transition.

the PM side due to substantially larger hybridization, and once again, SC disappears. These results suggest that here the third f electron may have become selectively itinerant and thus is weakly correlated with the remaining two. It is tempting to ask about its connection to the residual value of γ_0 at $T \rightarrow 0$ and to m_0 for $T > T_c$.

In summary, our theoretical phase diagram reproduces the fundamental features observed experimentally in a semi-quantitative manner. Within the doubly degenerate Anderson lattice model in the statistically consistent renormalized mean-field approximation (SGA), we have analyzed in detail the coexisting FM1 and spin-triplet A_1 SC phase, keeping in mind the experimental results for UGe_2 . We also obtained indirect evidence for an orbital-selective Mott-type delocalization of one of the $5f$ electrons at low temperature, which may be followed by its gradual localization in the high-temperature (Curie-Weiss) regime, leading to the U^{3+} magnetic configuration as exhibited by static magnetic susceptibility. Further specific material properties of UGe_2 and related systems can be drawn by incorporating the angular dependence of the hybridization, more realistic multiorbital structure, and the third dimension.

It would be interesting to incorporate, *renormalized* in this situation, quantum spin fluctuations into our SGA (renormalized-mean-field-theory-type picture). Such an approach would start from the effective Landau functional for fermions \mathcal{F} (see Appendix A) and the subsequent derivation of the corresponding functional involving magnetic-moment fluctuations as an intermediate step, which would allow us to include their contribution to the resultant free energy. Such a step, if executed successfully, would represent a decisive step beyond either the spin-fluctuation or the real-space-correlation approach. We should be able to see progress along these lines in the near future.

ACKNOWLEDGMENT

This work was supported by MAESTRO Grant No. DEC-2012/04/A/ST3/00342 from Narodowe Centrum Nauki (NCN).

APPENDIX A: STATISTICALLY CONSISTENT GUTZWILLER APPROXIMATION

Here we present technical details of the statistically consistent Gutzwiller approximation (SGA), as applied to the four-orbital model discussed in the main text. At zero temperature,

this variational technique reduces to the problem of minimizing the energy functional $E_G = \langle \Psi_G | \mathcal{H} | \Psi_G \rangle / \langle \Psi_G | \Psi_G \rangle$ with respect to the trial state $|\Psi_G\rangle = P_G |\Psi_0\rangle$ for fixed electron density. $|\Psi_0\rangle$ is an (*a priori* unknown) wave function describing the Fermi sea of free quasiparticles, whereas $\hat{P}_G = \prod_{il} \hat{P}_{Gi}^{(l)}$ denotes the Gutzwiller correlator [55]. Local correlators $\hat{P}_{Gi}^{(l)} = \sum_{\alpha} \lambda_{\alpha} |\alpha\rangle_{ii} \langle \alpha|$ adjust the weights of configurations $\alpha \in \{\emptyset, \uparrow, \downarrow, \uparrow\downarrow\}$ on each f orbital (indexed by l) at site i by means of coefficients λ_{α} multiplying projection operators $|\alpha\rangle_{ii} \langle \alpha|$. This is not the most general form of \hat{P}_G [56], but generalization makes the results less transparent and leads only to minor numerical corrections which may be safely disregarded. Evaluation of the expectation values with the correlated wave function is a nontrivial many-body problem. The latter can be substantially simplified by setting up a formal expansion about the limit of infinite lattice coordination, which is achieved by imposing the constraint $(\hat{P}_{Gi}^{(l)})^2 \equiv 1 + x \Pi_{\sigma} (\hat{n}_{i\sigma}^{f(l)} - n_{\sigma}^{f(l)})$ [57], so that all λ_{α} are now expressed in terms of a single variational parameter, x (we have introduced the notation $O \equiv \langle \hat{O} \rangle_0 \equiv \langle \Psi_0 | \hat{O} | \Psi_0 \rangle$ for the general operator \hat{O}). This approach was discussed in detail previously for the orbitally degenerate Hubbard and nondegenerate Anderson models [22,23,38,40].

We now focus on the four-orbital model, discussed in the main text, and calculate E_G by means of the Wick theorem, allowing for nonzero equal-spin pairing amplitudes $\langle \hat{f}_{i\sigma}^{(1)} \hat{f}_{i\sigma}^{(2)} \rangle_0$, orienting the magnetization direction along the z axis, and resorting to the Gutzwiller approximation by discarding the contributions irrelevant for infinite lattice coordination. In effect, we obtain

$$\begin{aligned}
 E_G \simeq & \sum_{ijl\sigma} t_{ij} \langle \hat{c}_{i\sigma}^{(l)\dagger} \hat{c}_{j\sigma}^{(l)} \rangle_0 + V \sum_{i\sigma} q_{\sigma} (\langle \hat{f}_{i\sigma}^{(l)\dagger} \hat{c}_{i\sigma}^{(l)} \rangle_0 + \text{c.c.}) \\
 & + \sum_{i\sigma} [U' g_{1\sigma} + (U' - J) g_{2\sigma}] |\langle \hat{f}_{i\sigma}^{(1)} \hat{f}_{i\sigma}^{(2)} \rangle_0|^2 \\
 & + \sum_i \left[-2J S_i^z f^{(1)} S_i^z f^{(2)} + \left(U' - \frac{J}{2} \right) n_i^{f(1)} n_i^{f(2)} \right] \\
 & + \epsilon^f \sum_{il} n_i^{f(l)} + U \sum_{il} \lambda_{\uparrow\downarrow}^2 n_{i\uparrow}^{f(l)} n_{i\downarrow}^{f(l)}, \quad (\text{A1})
 \end{aligned}$$

where the renormalization factors are defined as

$$\begin{aligned}
 q_{\sigma} &= \lambda_{\emptyset} \lambda_{\sigma} + (\lambda_{\uparrow\downarrow} \lambda_{\bar{\sigma}} - \lambda_{\emptyset} \lambda_{\sigma}) n_{\bar{\sigma}}^{f(l)}, \\
 g_{1\sigma} &= 2(\lambda_{\uparrow\downarrow}^2 - \lambda_{\bar{\sigma}}^2) [\lambda_{\sigma}^2 + (\lambda_{\uparrow\downarrow}^2 - \lambda_{\bar{\sigma}}^2) n_{\bar{\sigma}}^{f(l)}] n_{\sigma}^{f(l)}, \\
 g_{2\sigma} &= (\lambda_{\uparrow\downarrow}^2 - \lambda_{\bar{\sigma}}^2)^2 (n_{\bar{\sigma}}^{f(l)})^2 + [\lambda_{\sigma}^2 + (\lambda_{\uparrow\downarrow}^2 - \lambda_{\bar{\sigma}}^2) n_{\bar{\sigma}}^{f(l)}]^2. \quad (\text{A2})
 \end{aligned}$$

The SGA method maps the original many-body problem onto the task of calculating an effective Landau functional $\mathcal{F} = -\beta^{-1} \ln \text{Tr} \exp(-\beta \mathcal{H}_{\text{eff}})$ evaluated with the effective one-body Hamiltonian $\mathcal{H}_{\text{eff}} = E_G(\{P_{\gamma}, x\}) - \mu N_e + \sum_{\gamma} \lambda_{\gamma} (P_{\gamma} - P_{\gamma})$, where N_e is the total number of electrons in the system, γ runs over bilinear \hat{P}_{γ} composed of creation and annihilation operators, and λ_{γ} are Lagrange multipliers ensuring that P_{γ} obtained from optimization of \mathcal{F} and the Bogolubov-de Gennes equations coincide. The values of parameters are determined from the equations $\partial_{P_{\gamma}} \mathcal{F} = 0$, $\partial_x \mathcal{F} = 0$, and $\partial_{\lambda_{\gamma}} \mathcal{F} = 0$. Additionally, the value of the chemical potential μ

is fixed by electron density. Note that the original variational problem is well posed at $T = 0$, whereas the SGA formulation is applicable also for $T > 0$. One can argue (for the general coordination number) that for $T \rightarrow 0$ optimization of \mathcal{F} with \mathcal{H}_{eff} yields the variational minimum of E_G within the improved Gutzwiller approximation [31], whereas for $T > 0$ it reflects the thermodynamics of projected quasiparticles [58].

The explicit form of the effective Hamiltonian reads

$$\mathcal{H}_{\text{eff}} = \sum_{\mathbf{k}, \sigma} \Psi_{\mathbf{k}\sigma}^\dagger \begin{pmatrix} \epsilon_{\mathbf{k}} & 0 & q_\sigma V & 0 \\ 0 & -\epsilon_{\mathbf{k}} & 0 & -q_\sigma V \\ q_\sigma V & 0 & \epsilon_\sigma^f & \Delta_{\sigma\sigma}^{ff} \\ 0 & -q_\sigma V & \Delta_{\sigma\sigma}^{ff} & -\epsilon_\sigma^f \end{pmatrix} \Psi_{\mathbf{k}\sigma} + E_0, \quad (\text{A3})$$

where $\Psi_{\mathbf{k}\sigma}^\dagger = (\hat{c}_{\mathbf{k}\sigma}^{(1)\dagger}, \hat{c}_{-\mathbf{k}\sigma}^{(2)}, \hat{f}_{\mathbf{k}\sigma}^{(1)\dagger}, \hat{f}_{-\mathbf{k}\sigma}^{(2)})$, $\epsilon_{\mathbf{k}} = 2t[\cos(k_x) + \cos(k_y)] + 4t'\cos(k_x)\cos(k_y) - \mu$ is the conduction band dispersion,

$$\Delta_{\sigma\sigma}^{ff} = [g_{1\sigma}U' + g_{2\sigma}(U' - J)] \langle \hat{f}_{i\sigma}^{(1)} \hat{f}_{i\sigma}^{(2)} \rangle_0 \quad (\text{A4})$$

denotes the f - f superconducting gap parameter,

$$\begin{aligned} \epsilon_\sigma^f &= \frac{\partial E_G}{\partial n_{i\sigma}^{f(1)}} = \epsilon^f + U\lambda_{\uparrow\downarrow}^2 n_{i\bar{\sigma}}^{f(1)} + (U' - J)n_{i\sigma}^{f(2)} + U'n_{i\bar{\sigma}}^{f(2)} \\ &+ \left(\frac{\partial q_{\bar{\sigma}}}{\partial n_{i\sigma}^{f(1)}} V \sum_l \langle \hat{f}_{i\bar{\sigma}}^{(l)\dagger} \hat{c}_{i\bar{\sigma}}^{(l)} \rangle_0 + \text{c.c.} \right) \\ &+ \left(\frac{\partial g_{1\bar{\sigma}}}{\partial n_{i\sigma}^{f(1)}} U' + \frac{\partial g_{2\bar{\sigma}}}{\partial n_{i\sigma}^{f(1)}} (U' - J) \right) \left| \langle \hat{f}_{i\bar{\sigma}}^{(1)} \hat{f}_{i\bar{\sigma}}^{(2)} \rangle_0 \right|^2 - \mu \end{aligned} \quad (\text{A5})$$

is the renormalized f -orbital energy, and $E_0 \equiv E_G(\{P_\gamma, x\}) - \mu N_e - \sum_\gamma \lambda_\gamma P_\gamma$ is a remainder proportional to unity. Note that the entries for \mathcal{H}_{eff} have been obtained from one condition, $\partial_{P_\gamma} \mathcal{F} = 0$, and are given in an explicit form.

Since the effective Hamiltonian (A3) can be diagonalized analytically, with the eigenvalues

$$E_{\mathbf{k}\sigma}^{(\lambda)} = \pm \sqrt{q_\sigma^2 V^2 + \frac{1}{2}[(\Delta_{\sigma\sigma}^{ff})^2 + (\epsilon_\sigma^f)^2 + \epsilon_{\mathbf{k}}^2]} \pm \frac{1}{2} \sqrt{[(\Delta_{\sigma\sigma}^{ff})^2 + (\epsilon_\sigma^f)^2 - \epsilon_{\mathbf{k}}^2]^2 + 4q_\sigma^2 V^2 [(\Delta_{\sigma\sigma}^{ff})^2 + (\epsilon_{\mathbf{k}} + \epsilon_\sigma^f)^2]}, \quad (\text{A6})$$

one can express the gap $\Delta_{\mathbf{k}}$ in the projected quasiparticle spectrum in terms of the gap parameter $\Delta_{\sigma\sigma}^{ff}$. We get the formula

$$\Delta_{\mathbf{k}}^2 = \frac{\epsilon_{\mathbf{k}}^2}{(\epsilon_{\mathbf{k}} + \epsilon_\sigma^f)^2} (\Delta_{\sigma\sigma}^{ff})^2 + o[(\Delta_{\sigma\sigma}^{ff})^2], \quad (\text{A7})$$

valid for wave vectors located on the Fermi surface calculated in the normal state. Note that the gap is expressed solely in terms of the f - f pairing amplitude (even though f - c and c - c amplitudes are, in general, nonzero due to the hybridization effects) and scaled by the \mathbf{k} -dependent factor. This justifies using $\Delta_{\sigma\sigma}^{ff}$ as the quantity characterizing the overall SC properties of the system.

APPENDIX B: NUMERICAL PROCEDURE

The system of equations $\partial_{P_\gamma} \mathcal{F} = 0$, $\partial_x \mathcal{F} = 0$, and $\partial_{\lambda_\gamma} \mathcal{F} = 0$ has been solved by means of GNU Scientific Library. Numerical accuracy for the dimensionless density matrix elements was chosen in the range 10^{-8} – 10^{-9} , depending on the model parameters. We work in the thermodynamic limit with number of lattice sites $N \rightarrow \infty$ by performing Brillouin-zone integration in all equations. Technically, keeping N finite but large speeds up the calculations in a highly parallel setup. However, the calculated superconducting gap parameters range from $\sim 10^{-4}|t|$ down to $\sim 10^{-9}|t|$, which raises the question of the impact of the finite-size effects on the SC state. We can estimate the latter by referring to the Anderson criterion [59] $\Delta_{\sigma\sigma}^{ff} \sim d$, where $d \sim W/N$ is the typical spacing between discrete energy levels (W approximately equal to several $|t|$ denotes bandwidth scale, and N is the number of lattice sites). To achieve the desired accuracy, one would thus need to consider lattices with $> 10^{10}$ sites. This rationalizes our choice

to use adaptive integration and work directly with an infinite system.

The convergence properties of our computational scheme for the parameters corresponding to the A , A_1 , and A_2 phases are summarized in Figs. 6(a)–6(c). Only the SC amplitudes are displayed (connected points); the dashed lines mark the target numerical accuracy set in our code (note that the accuracy varies at the initial stage of the procedure due to drift of the renormalization factors). In each case, we performed a few warm-up iterations with imposed nonzero values of the SC gap parameters, symmetry-breaking external magnetic field, and finite temperature. This initial phase is seen in Fig. 6 as a plateau for fewer than ten iterations. Subsequently, the auxiliary fields were turned off, and the system was allowed to relax. For the A phase (zero total magnetization and $\Delta_{\uparrow\uparrow}^{ff} = \Delta_{\downarrow\downarrow}^{ff}$) and for the smallest gap amplitudes, we have executed the iterative procedure in different setups multiple times to verify the solutions. Two runs are marked in Fig. 6(a) by blue and green. In Figs. 6(b) and 6(c) green and purple lines show (now inequivalent) spin-down and spin-up amplitudes for the A_1 and A_2 phases. The S-shaped iteration dependence of $\Delta_{\uparrow\uparrow}^{ff}$ in Fig. 6(b) may be attributed to the proximity to the first-order FM2 + $A_2 \rightarrow$ FM1 + A_1 transition. The initial upturn of $\Delta_{\uparrow\uparrow}^{ff}$ is reminiscent of the behavior observed for the A_2 state [see Fig. 6(c)]. After the 25th iteration, however, the system switches to another attractor, and $\Delta_{\uparrow\uparrow}^{ff}$ is exponentially suppressed to quickly attain the numerical zero (A_1 phase).

APPENDIX C: DETERMINATION OF THE PHASE DIAGRAM

In Fig. 7(a) we plot the energies of the FM2 + A_2 and FM1 + A_1 phases near the metamagnetic transition for $J/|t| = 1.1$, $U/|t| = 3.5$, $t'/|t| = 0.25$, and $\epsilon^f/|t| = -4$ (the

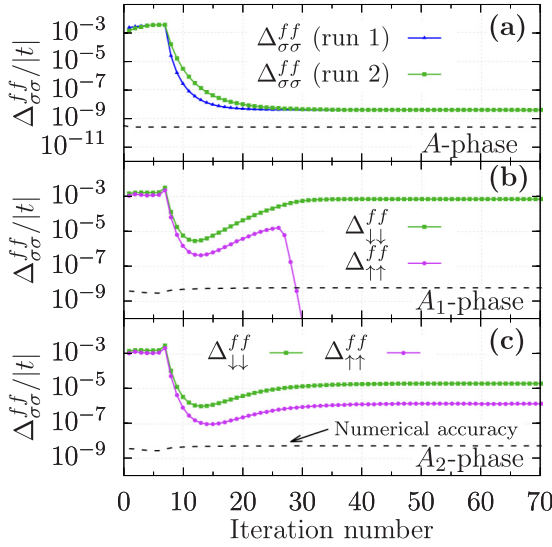


FIG. 6. Convergence properties of the solutions for the A, A_1 , and A_2 SC phases as a function of the iteration number. The values of hybridization are (a) $V/t \approx 3.0982$ (PM + A phase), (b) $V/t \approx 1.264$ (FM1 + A_1 phase just above the FM2 + $A_2 \rightarrow$ FM1 + A_1 transition), and (c) $V/t \approx 1.254$ (FM2 + A_2 phase just below the FM2 + $A_2 \rightarrow$ FM1 + A_1 transition). The remaining parameters are the same as in the main text. (a) shows two independent runs for the equivalent $\Delta_{\uparrow\uparrow}^{ff} = \Delta_{\downarrow\downarrow}^{ff}$ gap components. (b) and (c) The single run for two (inequivalent) gap parameters. The horizontal dashed lines mark the numerical accuracy.

same parameters used to plot Fig. 1). The solid lines are quadratic fits to the data in the respective phases. The phase-transition point V_{PT} corresponds to the crossing of the lines (marked by the vertical dashed lines). Note that the lines cross at a nonzero angle, which is indicative of the first-order transition. Similarly, in Fig. 7(b) the energies near the FM1 + A_1 and PM + A phase boundary are shown. In Figs. 7(c) and 7(d) we plot the difference between extrapolated energies on

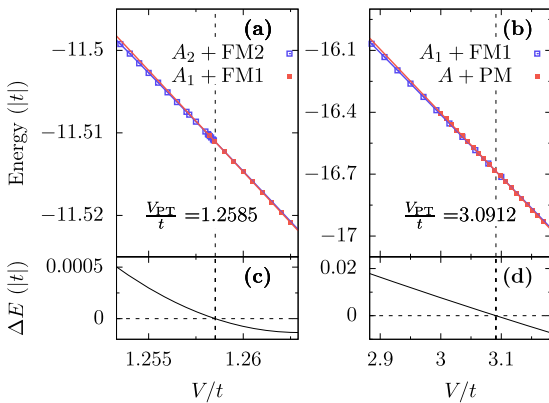


FIG. 7. Crossing of the energies near (a) FM2 + $A_2 \rightarrow$ FM1 + A_1 and (b) FM1 + $A_1 \rightarrow$ PM + A transition for $U/|t| = 3.5$. (c) and (d) The energy differences ΔE between extrapolated energies on both sides of the respective phase transitions. The latter become zero at the transition point, denoted as V_{PT} , and are displayed in the plot. Model parameters coincide with those used in Fig. 1.

TABLE I. Variational ground-state energies for $U/|t| = 3.5$ and $V/t = 1.32$, $t'/|t| = 0.25$, $\epsilon^f/|t| = -4$, $n^{\text{tot}} = 3.25$, and selected values of Hund's coupling J . Here E_{FM1} is the energy of the FM1 phase with SC suppressed, and $E_{\text{FM1}+A_1}$ refers to the FM1 phase coexisting with the A_1 -type SC. The condensation energy $E_c \equiv E_{\text{FM1}} - E_{\text{FM1}+A_1}$ is also supplied. The numerical accuracy of the energy difference is of the order of 2×10^{-8} .

$J/ t $	$E_{\text{FM1}}/ t $	$E_{\text{FM1}+A_1}/ t $	$10^4 \times E_c/ t $
1.10	-11.663 459 37	-11.663 459 39	0.0003
1.15	-11.796 917 55	-11.796 917 77	0.0022
1.20	-11.934 039 49	-11.934 041 79	0.0230
1.25	-12.074 935 82	-12.074 951 80	0.1598
1.30	-12.219 724 82	-12.219 802 79	0.7797
1.35	-12.368 534 05	-12.368 822 15	2.8810
1.40	-12.521 501 70	-12.522 354 69	8.5299

both sides of the transitions. The difference becomes zero at the transition point.

For the sake of completeness, in Table I we present the analysis of A_1 -type SC phase stability for $U/|t| = 3.5$, $V/t = 1.32$, $t'/|t| = 0.25$, $\epsilon^f/|t| = -4$, and variable Hund's coupling $J/|t| = 1.1-1.4$. Here E_{FM1} is the energy of the FM1 phase with SC suppressed, and $E_{\text{FM1}+A_1}$ refers to the FM1 phase coexisting with A_1 -type SC. The condensation energy $E_c \equiv E_{\text{FM1}} - E_{\text{FM1}+A_1}$ is positive for all considered values of hybridization, which illustrates the stable character of the SC state.

APPENDIX D: NONZERO-TEMPERATURE PROPERTIES

Within the SGA approach, one can also determine the finite-temperature properties of the system. In Fig. 8 we show explicitly the evolution of the gap parameter $\Delta_{\downarrow\downarrow}^{ff}$ and electronic specific heat across the SC transition for $U/|t| = 3.5$, $J/|t| = 1.1$, $V/t = 1.3$, $t'/|t| = 0.25$, and $\epsilon^f = -4$. For this set of parameters the system is close to the FM2 \rightarrow FM1 transition, where SC is the most pronounced (see Fig. 1). For the specific choice $|t| = 0.5$ eV we obtain the SC transition temperature $T_{\text{SC}} \approx 0.92$ K, which is close to the values measured for high-quality UGe₂ samples. On the other hand, we do not

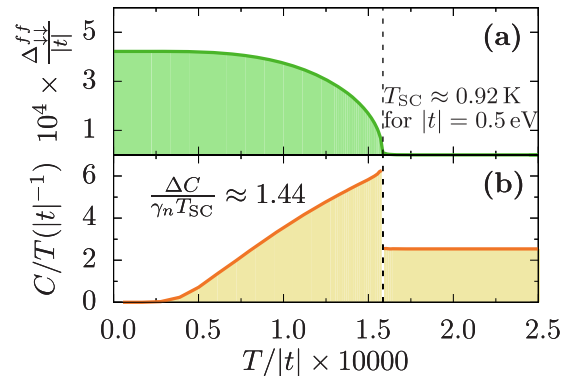


FIG. 8. Temperature dependence of (a) the gap parameter $\Delta_{\downarrow\downarrow}^{ff}$ and (b) electronic specific heat for $U/|t| = 3.5$, $J/|t| = 1.1$, $V/t = 1.3$, $\epsilon^f/|t| = -4$, $t'/|t| = 0.25$, and $n^{\text{tot}} = 3.25$.

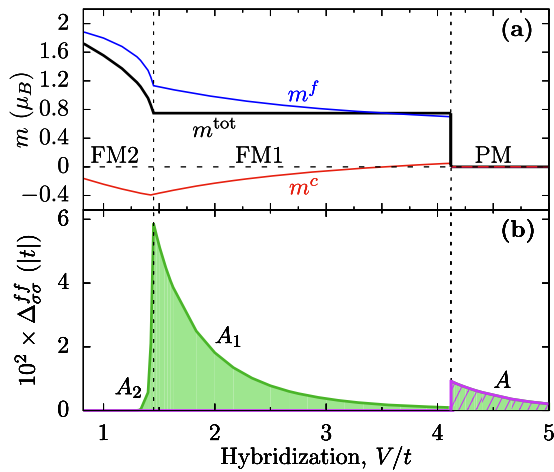


FIG. 9. Phase diagram for $U/|t| = 4$, $J/|t| = 1.6$, $t'/|t| = 0.25$, temperature $T/|t| = 10^{-8}$, and $n^{\text{tot}} = 3.25$. (a) Total magnetic moment (black line) and f - and c -electron magnetizations (blue and red lines, respectively). (b) Superconducting gap parameters $\Delta_{\sigma\sigma}^{ff}$ (green shading) and $\Delta_{\uparrow\downarrow}^{ff}$ (purple shading).

get the residual C/T for $T \rightarrow 0$ as observed for UGe_2 . This is likely due to the more complex electronic structure, not included in the minimal four-orbital model considered here, e.g., by the third $5f$ electron, which provides the orbital-selective delocalized state, as discussed in the main text. This conjecture is substantiated by the fact that if we subtract the

residual γ_0 from the measured Sommerfeld coefficient γ_n , then $\Delta C/(\gamma_n - \gamma_0)/T_{\text{SC}} \simeq 0.97$ [51], i.e., not too far from the value displayed in Fig. 8(b), which, in turn, is close to the BCS value of 1.43. [60]

APPENDIX E: PHASE DIAGRAM IN THE REGIME OF LARGE HUND'S COUPLING

For the parameters taken in the main text, the A -phase gaps turn out to be of the order of $\Delta_{\sigma\sigma}^{ff}/|t| \sim 10^{-9}$, which sets the critical temperature scale at the level of 0.01 mK for $|t| \sim 1$ eV. This raises a question about, limited to special situations, the observability of the A state. Here we show that the A phase may become substantially enhanced in the regime of strong correlations and large Hund's coupling. In Fig. 9 we show the hybridization dependence of the magnetization and SC gaps for $U/|t| = 4$, $J/|t| = 1.6$, $t'/|t| = 0.25$, $\epsilon^f/|t| = -4$, and temperature $T/|t| = 10^{-8}$. The general structure of the phase diagram remains unchanged, but the ratio of the gap parameters in the A and A_1 phases is now enhanced by five orders of magnitude relative to the situation considered previously in the UGe_2 case. However, this last feature suggests that an A -like phase could emerge in systems more strongly correlated than UGe_2 . Also, now the A_1 phase is not concentrated in a narrow region around the metamagnetic transition but spreads over the entire FM1 region of the phase diagram. This is not consistent with the low-temperature specific-heat data [51] for UGe_2 exhibiting a narrow peak around the FM2 \rightarrow FM1 transition. This fact justified our choice of smaller $U/|t| = 3.5$ and $J/|t| = 1.1$.

- [1] S. S. Saxena, P. Agarwal, K. Ahilan, F. M. Grosche, R. K. W. Haselwimmer, M. J. Steiner, E. Pugh, I. R. Walker, S. R. Julian, P. Monthoux, G. G. Lonzarich, A. Huxley, I. Sheikin, D. Braithwaite, and J. Flouquet, Superconductivity on the border of itinerant-electron ferromagnetism in UGe_2 , *Nature (London)* **406**, 587 (2000).
- [2] N. Tateiwa, T. C. Kobayashi, K. Hanazono, K. Amaya, Y. Haga, R. Settai, and Y. Onuki, Pressure-induced superconductivity in a ferromagnet UGe_2 , *J. Phys.: Condens. Matter* **13**, L17 (2001).
- [3] C. Pfleiderer and A. D. Huxley, Pressure Dependence of the Magnetization in the Ferromagnetic Superconductor UGe_2 , *Phys. Rev. Lett.* **89**, 147005 (2002).
- [4] A. Huxley, I. Sheikin, E. Ressouche, N. Kernavanois, D. Braithwaite, R. Calemczuk, and J. Flouquet, UGe_2 : A ferromagnetic spin-triplet superconductor, *Phys. Rev. B* **63**, 144519 (2001).
- [5] D. Aoki, A. Huxley, E. Ressouche, D. Braithwaite, J. Flouquet, J.-P. Brison, E. Lhotel, and C. Paulsen, Coexistence of superconductivity and ferromagnetism in URhGe , *Nature (London)* **413**, 613 (2001).
- [6] N. T. Huy, A. Gasparini, D. E. de Nijs, Y. Huang, J. C. P. Klaasse, T. Gortenmulder, A. de Visser, A. Hamann, T. Görlach, and H. v. Löhneysen, Superconductivity on the Border of Weak Itinerant Ferromagnetism in UCoGe , *Phys. Rev. Lett.* **99**, 067006 (2007).
- [7] T. C. Kobayashi, S. Fukushima, H. Hidaka, H. Kotegawa, T. Akazawa, E. Yamamoto, Y. Haga, R. Settai, and Y. Onuki, Pressure-induced superconductivity in ferromagnet UIr without inversion symmetry, *Phys. B (Amsterdam, Neth.)* **378-380**, 355 (2006).
- [8] C. Pfleiderer, Superconducting phases of f -electron compounds, *Rev. Mod. Phys.* **81**, 1551 (2009).
- [9] D. Aoki and J. Flouquet, Ferromagnetism and superconductivity in uranium compounds, *J. Phys. Soc. Jpn.* **81**, 011003 (2012).
- [10] A. P. Mackenzie and Y. Maeno, The superconductivity of Sr_2RuO_4 and the physics of spin-triplet pairing, *Rev. Mod. Phys.* **75**, 657 (2003).
- [11] A. D. Huxley, Ferromagnetic superconductors, *Phys. C (Amsterdam, Neth.)* **514**, 368 (2015).
- [12] P. Coleman, Superconductivity: On the verge of magnetism, *Nature (London)* **406**, 580 (2000).
- [13] K. G. Sandeman, G. G. Lonzarich, and A. J. Schofield, Ferromagnetic Superconductivity Driven by Changing Fermi Surface Topology, *Phys. Rev. Lett.* **90**, 167005 (2003).
- [14] T. Hattori, Y. Ihara, Y. Nakai, K. Ishida, Y. Tada, S. Fujimoto, N. Kawakami, E. Osaki, K. Deguchi, N. K. Sato, and I. Satoh, Superconductivity Induced by Longitudinal Ferromagnetic Fluctuations in UCoGe , *Phys. Rev. Lett.* **108**, 066403 (2012).
- [15] Y. Tada, S. Fujimoto, N. Kawakami, T. Hattori, Y. Ihara, K. Ishida, K. Deguchi, N. K. Sato, and I. Satoh, Spin-triplet superconductivity induced by longitudinal ferromagnetic fluctuations in UCoGe : Theoretical aspect, *J. Phys.: Conf. Series* **449**, 012029 (2013).
- [16] B. Wu, G. Bastien, M. Taupin, C. Paulsen, L. Howald, D. Aoki, and J.-P. Brison, Pairing mechanism in the ferromagnetic superconductor UCoGe , *Nat. Commun.* **8**, 14480 (2017).

- [17] N. K. Sato, K. Deguchi, K. Imura, N. Kabeya, N. Tamura, and K. Yamamoto, Correlation of Ferromagnetism and Superconductivity in UCoGe, in *International Conference on Magnetic Materials (ICMM-2010)*, edited by A. Ghoshray, B. Bandyopadhyay, and C. Mazumdar, AIP Conf. Proc. No. 1347 (AIP, New York, 2011), p. 132.
- [18] J. Spałek, Spin-triplet superconducting pairing due to local Hund's rule and Dirac exchange, *Phys. Rev. B* **63**, 104513 (2001).
- [19] A. Klejnberg and J. Spałek, Hund's rule coupling as the microscopic origin of the spin-triplet pairing in a correlated and degenerate band system, *J. Phys.: Condens. Matter* **11**, 6553 (1999).
- [20] J. Spałek, P. Wróbel, and W. Wójcik, Coexistence of Spin-Triplet Superconductivity and Ferromagnetism Induced by the Hund's Rule Exchange, in *Ruthenate and Rutheno-Cuprate Materials*, edited by C. Noce, A. Vecchione, M. Cuoco, and A. Romano, Lecture Notes in Physics Vol. 603 (Springer, Berlin, 2002), pp. 60–75.
- [21] J. Spałek and M. Zegrodnik, Spin-triplet paired state induced by Hund's rule coupling and correlations: A fully statistically consistent Gutzwiller approach, *J. Phys.: Condens. Matter* **25**, 435601 (2013).
- [22] M. Zegrodnik, J. Spałek, and J. Büneemann, Coexistence of spin-triplet superconductivity with magnetism within a single mechanism for orbitally degenerate correlated electrons: Statistically consistent Gutzwiller approximation, *New J. Phys.* **15**, 073050 (2013).
- [23] M. Zegrodnik, J. Büneemann, and J. Spałek, Even-parity spin-triplet pairing by purely repulsive interactions for orbitally degenerate correlated fermions, *New J. Phys.* **16**, 033001 (2014).
- [24] J. E. Han, Spin-triplet s -wave local pairing induced by Hund's rule coupling, *Phys. Rev. B* **70**, 054513 (2004).
- [25] S. Hoshino and P. Werner, Superconductivity from Emerging Magnetic Moments, *Phys. Rev. Lett.* **115**, 247001 (2015).
- [26] X. Dai, Z. Fang, Y. Zhou, and F.-C. Zhang, Even Parity, Orbital Singlet, and Spin Triplet Pairing for Superconducting LaFeAsO_{1-x}F_x, *Phys. Rev. Lett.* **101**, 057008 (2008).
- [27] P. W. Anderson, P. A. Lee, M. Randeria, T. M. Rice, N. Trivedi, and F. C. Zhang, The physics behind high-temperature superconducting cuprates: The 'plain vanilla' version of RVB, *J. Phys.: Condens. Matter* **16**, R755 (2004).
- [28] B. Edegger, V. N. Muthukumar, and C. Gros, Gutzwiller-RVB theory of high-temperature superconductivity: Results from renormalized mean-field theory and variational Monte Carlo calculations, *Adv. Phys.* **56**, 927 (2007).
- [29] M. Ogata and H. Fukuyama, The t - J model for the oxide high- T_c superconductors, *Rep. Prog. Phys.* **71**, 036501 (2008).
- [30] J. Jędrak and J. Spałek, Renormalized mean-field t - J model of high- T_c superconductivity: Comparison to experiment, *Phys. Rev. B* **83**, 104512 (2011).
- [31] J. Kaczmarczyk, J. Büneemann, and J. Spałek, High-temperature superconductivity in the two-dimensional t - J model: Gutzwiller wavefunction solution, *New J. Phys.* **16**, 073018 (2014).
- [32] J. Spałek, M. Zegrodnik, and J. Kaczmarczyk, Universal properties of high-temperature superconductors from real-space pairing: t - J - U model and its quantitative comparison with experiment, *Phys. Rev. B* **95**, 024506 (2017).
- [33] O. Bodensiek, R. Žitko, M. Vojta, M. Jarrell, and T. Pruschke, Unconventional Superconductivity from Local Spin Fluctuations in the Kondo Lattice, *Phys. Rev. Lett.* **110**, 146406 (2013).
- [34] O. Howczak, J. Kaczmarczyk, and J. Spałek, Pairing by Kondo interaction and magnetic phases in the Anderson-Kondo lattice model: Statistically consistent renormalized mean-field theory, *Phys. Status Solidi B* **250**, 609 (2013).
- [35] W. Wu and A.-M.-S. Tremblay, d -Wave Superconductivity in the Frustrated Two-Dimensional Periodic Anderson Model, *Phys. Rev. X* **5**, 011019 (2015).
- [36] M. M. Wysokiński, J. Kaczmarczyk, and J. Spałek, Correlation-driven d -wave superconductivity in Anderson lattice model: Two gaps, *Phys. Rev. B* **94**, 024517 (2016).
- [37] N. Tateiwa, J. Pospíšil, Y. Haga, H. Sakai, T. D. Matsuda, and E. Yamamoto, Itinerant ferromagnetism in actinide $5f$ -electron systems: Phenomenological analysis with spin fluctuation theory, *Phys. Rev. B* **96**, 035125 (2017).
- [38] M. M. Wysokiński, M. Abram, and J. Spałek, Ferromagnetism in UGe₂: A microscopic model, *Phys. Rev. B* **90**, 081114 (2014).
- [39] M. M. Wysokiński, M. Abram, and J. Spałek, Criticalities in the itinerant ferromagnet UGe₂, *Phys. Rev. B* **91**, 081108 (2015).
- [40] M. Abram, M. M. Wysokiński, and J. Spałek, Tricritical wings in UGe₂: A microscopic interpretation, *J. Magn. Magn. Mater.* **400**, 27 (2016).
- [41] J. C. Wheatley, Experimental properties of superfluid ³He, *Rev. Mod. Phys.* **47**, 415 (1975).
- [42] P. W. Anderson and W. F. Brinkman, Anisotropic Superfluidity in ³He: A Possible Interpretation of Its Stability as a Spin-Fluctuation Effect, *Phys. Rev. Lett.* **30**, 1108 (1973).
- [43] W. F. Brinkman, J. W. Serene, and P. W. Anderson, Spin-fluctuation stabilization of anisotropic superfluid states, *Phys. Rev. A* **10**, 2386 (1974).
- [44] D. Fay and J. Appel, Coexistence of p -state superconductivity and itinerant ferromagnetism, *Phys. Rev. B* **22**, 3173 (1980).
- [45] P. Monthoux and G. G. Lonzarich, p -wave and d -wave superconductivity in quasi-two-dimensional metals, *Phys. Rev. B* **59**, 14598 (1999).
- [46] A. B. Shick and W. E. Pickett, Magnetism, Spin-Orbit Coupling, and Superconducting Pairing in UGe₂, *Phys. Rev. Lett.* **86**, 300 (2001).
- [47] A. B. Shick, V. Janiš, V. Drchal, and W. E. Pickett, Spin and orbital magnetic state of UGe₂ under pressure, *Phys. Rev. B* **70**, 134506 (2004).
- [48] R. Troć, Z. Gajek, and A. Pikul, Dualism of the $5f$ electrons of the ferromagnetic superconductor UGe₂ as seen in magnetic, transport, and specific-heat data, *Phys. Rev. B* **86**, 224403 (2012).
- [49] M. Samsel-Czekała, M. Werwiński, A. Szajek, G. Chełkowska, and R. Troć, Electronic structure of UGe₂ at ambient pressure: Comparison with x-ray photoemission spectra, *Intermetallics* **19**, 1411 (2011).
- [50] J. Spałek, D. K. Ray, and M. Acquarone, A hybridized basis for simple band structures, *Solid State Commun.* **56**, 909 (1985).
- [51] N. Tateiwa, T. C. Kobayashi, K. Amaya, Y. Haga, R. Settai, and Y. Ōnuki, Heat-capacity anomalies at T_{sc} and T^* in the ferromagnetic superconductor UGe₂, *Phys. Rev. B* **69**, 180513(R) (2004).
- [52] M. Fidrzyśiak, E. Kądziaława-Major, and J. Spałek (unpublished).

- [53] Z. P. Yin, K. Haule, and G. Kotliar, Kinetic frustration and the nature of the magnetic and paramagnetic states in iron pnictides and iron chalcogenides, *Nat. Mater.* **10**, 932 (2011).
- [54] A. Harada, S. Kawasaki, H. Mukuda, Y. Kitaoka, Y. Haga, E. Yamamoto, Y. Ōnuki, K. M. Itoh, E. E. Haller, and H. Harima, Experimental evidence for ferromagnetic spin-pairing superconductivity emerging in UGe_2 : A ^{73}Ge -nuclear-quadrupole-resonance study under pressure, *Phys. Rev. B* **75**, 140502(R) (2007).
- [55] M. C. Gutzwiller, Effect of Correlation on the Ferromagnetism of Transition Metals, *Phys. Rev. Lett.* **10**, 159 (1963).
- [56] P. Kubiczek, Spin-triplet pairing in orbitally degenerate Anderson lattice model, M.Sc. thesis, Jagiellonian University, 2016.
- [57] J. Bünemann, T. Schickling, and F. Gebhard, Variational study of Fermi surface deformations in Hubbard models, *Europhys. Lett.* **98**, 27006 (2012).
- [58] M. Fidrysiak, M. Zegrodnik, and J. Spałek (unpublished).
- [59] P. W. Anderson, Theory of dirty superconductors, *J. Phys. Chem. Solids* **11**, 26 (1959).
- [60] R. Kishore and S. Lamba, Specific heat jump in BCS superconductors, *Eur. Phys. J. B* **8**, 161 (1999).